JOURNAL OF CATALYSIS 115, 120–131 (1989)

Chemistry of Supported Ru: CO-Induced Oxidation of Ru at 310 K

JOHN L. ROBBINS

Exxon Corporate Research Science Labs, Route 22, East, Annandale, New Jersey 08801

Received April 6, 1988; revised July 5, 1988

Infrared spectra of CO on reduced titania-supported Ru show three bands at 2060, 2085, and 2140 cm^{-1}. The first band saturates almost instantly in excess CO and exhibits coverage-dependent frequencies at subsaturation which are consistent with its assignment to CO in on-top sites on the anticipated Ru crystallites. The latter two bands grow slowly as a pair in several Torr CO at 310 K, and their growth rate is accelerated at 400 K. IR spectra measured in mixtures of isotopically labeled CO show the two high-frequency bands represent coupled vibrations of an $Ru(CO)_x$ ($x > 2$) species. The observed frequencies correlate with those expected for a Ru(II) species and XPS shows that a fraction of the zero-valent Ru present on a reduced sample is converted to a higher valent species upon exposure to CO at 310 K. We therefore assign the 2085- and 2140-cm^{-1} IR bands to $(TiO)_2Ru(CO)_3$ surface species. We also propose these species form via an oxidative fragmentation reaction involving zero-valent Ru, CO, and surface hydroxyls on the support.

INTRODUCTION

The unusual CO chemisorption properties of support Ru particles have been documented by several techniques. In volumetric uptake experiments, CO/M ratios greater than 2 and CO_{ads}/H_{ads} ratios greater than 3 have been reported for highly dispersed samples (*1–4*). Infrared studies of chemisorbed CO show several types of adsorption sites are present. The spectra of CO on well-reduced and poorly dispersed materials are typically dominated by a coverage-dependent band centered at 2040 to 2060 cm^{-1} under conditions of CO saturation (*5–21*). In accord with vibrational studies of CO on single crystal Ru(001) surfaces, this band is assigned to CO in on-top (or terminal) sites on the anticipated Ru crystallites (*22*). According to one report, this band shifts in frequency from 2090 to 2050 cm^{-1} as the Ru particle size varies from 10 to 70 Å on alumina supports (*2*).

Of primary interest to us here are the higher frequency features often observed near 2140 and 2080 cm^{-1}. A pair of these bands has been observed for CO on silica- (*3, 5–9, 12, 16*), alumina- (*2, 12*), and zeolite- (*17*) supported Ru, but not for CO on Ru single crystals (*23*). Phenomenologically, the intensity of these high-frequency (HF) bands on supported systems appears to increase, relative to the intensity of the 2060-cm^{-1} band, as the metal dispersion increases. This has led to the postulate that the HF bands represent symmetric and antisymmetric stretching modes of di- or tricarbonyl sites on the edges or corners of small Ru crystallites (*2, 3*). Another model ascribes the HF bands to CO on Ru modified by an electronegative element such as Cl or O (*5, 6*). In fact, recent EELS and IRAS studies show CO on O-modified Ru(001) gives rise to a single IR band at 2080 cm^{-1} (*24*). Thus observed intensity near 2080 cm^{-1} for CO on supported catalysts may be due in part to incomplete reduction. Others have suggested the HF bands are due to COs bonded to Ru(II) or Ru(III) ions covalently bonded to oxygen atoms on the support surface (*5 11 12 14 17*). This assignment is based partly on the spectroscopic similarity of the observed HF bands and several well-known stable compounds such as $Ru_2(CO)_6Cl_4$, a dimeric Ru(II) complex with two bridging halogens.

0021-9517/89 $3.00

Numerous studies of Ru carbonyl cluster reactions with ceramic oxide surfaces show that a wide variety of grafted structures we refer to as $(\text{Support-O})_x\text{Ru}_n(\text{CO})_y$ are viable species with exceptional thermal stability (*14, 25*). These species are thought to form via a generalized redox reaction involving zero-valent Ru in the carbonyl cluster and support surface hydroxyl groups:

$$\text{Ru}_n(\text{CO})_z + nx\ \text{Support-O-H} = (\text{Support-O})_x\text{Ru}_n(\text{CO})_y + n/2\ \text{H}_2 + (z - y)\text{CO} \quad (1)$$

In this reaction, Ru is oxidized, hydroxyls are reduced to liberate hydrogen, and CO ligands are expelled to the extent that electron counting rules for stable molecular species require. Based on molecular analogies, reactions such as this can be expected to form a richly diverse series of structures. Monomeric, dimeric, trimeric, and polymeric Ru halocarbonyls with Ru in formal oxidation states of 2 and 3 have been structurally characterized (*26*). Each example exhibits a unique IR signature in the CO stretching region. IR spectra recorded during the course of these Ru carbonyl decompositions on oxide surfaces are quite complex, consisting of 10 or more discrete bands in the carbonyl region (*12, 14, 27–29*). The complexity of the observed spectra is not surprising in light of the many potentially stable species which might be anticipated to form on the basis of molecular analogy to known compounds. However, most of such studies reveal the development of a species with CO stretching frequencies near 2140 and 2080 cm^{-1} during the decomposition process. The IR spectral similarity of known molecular species (e.g., $\text{Ru}_2(\text{CO})_6\text{Cl}_4$)), stable entities formed during the thermal decomposition of $\text{Ru}_3(\text{CO})_{12}$ on oxides, and sites generated when CO is chemisorbed on reduced, supported Ru, suggest a common, electronically similar Ru species is present in all three cases.

With this as a structural paradigm, we have further investigated the surface species generated upon contact of CO with reduced titania-supported Ru. Our goals were two-fold. First we wanted to ascertain by spectroscopic and chemical methods whether or not the formulation $(\text{TiO})_x\text{Ru}(\text{CO})_n$ provides an adequate description of nonmetallic structures formed during the chemisorption reaction. Experimental results indicate that is the case. Second, we wanted to determine whether these sites are generated by addition of CO to cationic Ru sites which are resistant to reduction, or by chemical redox reactions of CO with metallic Ru and surface hydroxyl groups. The former case is exemplified by many first row transition metals which, at low metal loadings, form surface inorganic phases (metal aluminates, silicates, titanates, etc.) which are notoriously difficult to reduce in hydrogen even at temperatures above those required to reduce the bulk transition metal oxides. The latter case is best exemplified by the Rh/alumina system. Although EXAFS and thermogravimetric studies show Rh salts on alumina are readily reduced to metallic Rh particles in hydrogen at 250 to 300°C, infrared spectra of reduced materials exposed to CO at room temperature often exhibit bands at 2100 and 2030 cm^{-1} which are attributed to oxidized Al-O-Rh(CO)_2 sites. The ratio of these sites to metallic Rh(CO) sites increases with increasing Rh dispersion. Much evidence now indicates that these sites form when CO is introduced to the reduced metal system (*30–32*). The reaction:

$$\text{Rh}_n + 2n(\text{CO}) + n(\text{AlOH}) = n\ \text{Al-O-Rh(CO)}_2 + n/2\ \text{H}_2 \quad (2)$$

is currently thought responsible for this transformation. Qualitative thermochemical arguments show such a reaction may be exothermic if fewer than 5 Rh–Rh bonds are broken in the process (*30*). This situation exists for Rh atoms in small Rh particles and at the edges of larger ones. The thermochemical energies for metal–metal, metal–CO, and metal–O bonds are similar

for Rh and Ru, differing by no more than 5 kcal/mole each, so an analogous reaction may be possible for supported Ru (*33*).

Here we report evidence that oxidized $(TiO)_xRu(CO)_y$ species form spontaneously when well-reduced Ru/TiO_2 specimens are exposed to CO near room temperature. Infrared studies show these species may be distinguished from CO on metallic Ru crystallites by their differing lability with gas phase CO and reactivity toward oxygen. XPS shows addition of CO to the hydrogen reduced system at 300 K results in oxidation of some of the formerly zero-valent Ru. We propose that reactions like the one described above for Rh are responsible for this oxidation reaction.

EXPERIMENTAL

Materials

Two different Ru/TiO_2 samples were examined in the course of this study. Both were prepared using TiO_2 which was derived from a common lot of Degussa P-25 titania (64 m^2/g; 73% anatase, 27% rutile by XRD). For sample I, this titania was calcined for 2 h in flowing oxygen at 1120 K to afford XRD-pure rutile with a BET surface area of 10 m^2/g. For sample II, the Degussa support was calcined for 2 h at 1020 K. The product was a 50/50 mixture of anatase and rutile by XRD and had a BET surface area of 41 m^2/g. No significant IR spectral differences were observed for materials prepared from these two supports.

Ru was introduced by adding a weighed quantity of 8% $Ru(NO_3)_3$ solution (Engelhard; 99.9% Ru on metals basis) to a weighed amount of the titania suspended in rapidly stirred spectroscopic grade acetone. The solvent was allowed to evaporated in air with continuous stirring. For sample I, the powder was first dried in flowing oxygen for 20 h at 423 K. It was then first dried in flowing oxygen for 20 h at 423 K. It was then charged into a quartz tube, reduced in flowing 10% H_2 in He at 523 K (heating rate 2 K/min) for 12 h, flushed with pure CO at 300 K, and reduced again in the H_2/He for 6 h at 523 K (0.95% Ru). The reduced sample was flushed with N_2 at room temperature and then passivated by the slow diffusion of air through a capillary. For sample II, the air-dried impregnated powder was calcined in O_2 for 3 h at 523 K, and then reduced in flowing 10% H_2/He for 22 h at 523 K. The sample was passivated as described above (1.02% Ru). X-ray powder patterns and BET surface areas of the finished materials were indistinguishable from those of their respective supports. Hydrogen chemisorption measurements indicate that the Ru dispersion for samples I and II is 27% and 18%, respectively. For these measurements, the samples were reduced in quartz for 2 h at 548 K and then evacuated for 0.5 h at 623 K. The double isotherm method was employed. Using these values and Dalla Betta's assumptions for alumina-supported Ru, we calculate average hemispherical particle diameters of 30 Å for I and 45 Å for II. X-ray powder patterns of Ib and II show no discernible Ru reflections, suggesting particle sizes less than 60 Å. Electron microscopy was of little value in characterizing the metal particle size distribution. At a final magnification of 500,000, micrographs of I and II exhibit a profusion of 10- to 20-Å dark spots on the support surface. We originally attributed these to very small Ru particles, but the discrepancy between this result and the chemisorption data (which were measured in the non-SMSI state following low-temperature reduction) was a matter of some concern. A TEM study of the supports resolved the dilemma. Those micrographs displayed a similar profusion of 10- to 20-Å spots in the absence of Ru. We conclude that the support particles are highly textured with either warty protrubances or pits. Either feature can give rise to contrast images depending on phase conditions.

The H_2 and 10% H_2 in He used for reductions were initially >99.99% pure. Oxygen and H_2O contamination levels were reduced to ca. 1 ppm by passage through Matheson Gas Purifiers. He was passed

through a SGP purification cartridge and then 5-Å molecular sieves maintained at 77 K. Research purity CO (Matheson, less than 10 ppm O_2 and H_2O) and ^{13}C-enriched CO (Isotek; 99 atom% ^{13}C) were used for adsorption studies without further purification. *In situ* reductions were performed with a gas flow rate of 10 cm^3/min. For a typical IR sample this corresponds to a space velocity of 1700 h^{-1}.

Methods

Some of the IR spectra were recorded for pressed wafers of the powders inside an evacuable transmission IR cell sealed to a U-tube quartz reactor. This reactor and the associated vacuum and dosing manifolds were described previously (*31*). More recent studies were performed in a stainless steel IR cell/reactor of our own design. This low dead-volume reactor basically consists of a double-sided Mini-Conflat flange bored axially with a 15-mm hole to provide a light transmission path. Sixteen millimeter diameter sample wafers sit on step machined into this flange. Three holes radially drilled into the flange are brazed to lengths of $\frac{1}{16}$ in. stainless steel tubing. Two of these tubes are brazed to steel bellows valves to allow for gas inlet and outlets. The third tube accommodates a 0.01 in. diameter sheathed K thermocouple which records sample temperature. The thermocouple is sealed to the tube with Torr-Seal vacuum epoxy 6 in. away from heated reactor parts. Sapphire viewports on Mini-Conflat flanges (Varian or MDC) or CaF_2 plates on Mini-Conflat flanges (Harshaw) form a UHV seal to the central flange with Cu gaskets. The sapphire windows have a limitation in that they exhibit an IR transmission cutoff in the 1600- to 1650-cm^{-1} range. However, they have proven quite durable in withstanding rapid cycling (up to 30 K/min) from room temperature to 720 K without window fracture or the development of leaks at the window-to-flange seal. The CaF_2 windows cutoff at a much lower frequency (ca. 1050 cm^{-1}) but are more prone to fracture from thermal shock and to the development of leaks at the window/flange seal at temperatures greater than 620 K. In our experience the windows have never fractured from thermal shock when heated or cooled at less than 3.5 K/min between 270 and 680 K. Prolonged use of these windows above 620 K has resulted in leaks between the window and flange on several occasions. This is probably related to the fact that AgCl is used to form that seal. This material can cold flow at temperatures well below its melting point (690 K).

The assembled cell and valves are mounted on an Al stand which centers the transmission path in the IR beam. A cylindrical brass block slides onto the cell without blocking the IR beam. Three 80-W cartridge heaters slide into the brass block for cell heating. Temperature is controlled with a Valley Forge temperature programmer which heats and cools the apparatus at a specified rate. The cell attaches to a high vacuum/gas dosing manifold described before (*31*). The manifold is now equipped with a turbo-pumped UTI 100C quadrupole mass spectrometer for on line gas analysis. Exhaust gas from the cell is directed to an HP 5880 gas chromatograph via a heated transfer line for product analysis.

IR spectra were recorded on a Perkin-Elmer Model 684 grating spectrophotometer interfaced to a PE 3600 Data Station. Spectral slit widths of 6 to 8 cm^{-1} were employed in the 2300- to 1700-cm^{-1} region. The reference beam was not attenuated to compensate for support absorptions. Rather, spectra of reduced and outgassed wafers were averaged prior to admission of adsorbates to provide a background which could be subtracted later. Background and sample spectra were routinely averaged 16 times to enhance signal-to-noise ratios. Single scans (1 min each) were measured when spectra proved time dependent over a 5-min time scale.

XPS measurements were performed in a UHV chamber with *in situ* pretreatment capabilities that have been described (*34*).

Powder samples were pressed into a gold-plated holder which can be moved from a microreactor to the UHV chamber. The reported Ru $3d_{5/2}$ line positions are referenced to the Au $4f_{7/2}$ line (from the sample holder) at 83.8 eV. BET measurements, X-ray powder patterns, and Ru analyses were determined in our Analytical Laboratories.

We wish to make one final important comment before describing the experimental results. None of the spectra shown here represent CO chemisorbed on a wafer following its first reduction in H_2. In order to evaluate the influence of variations in sample pretreatment on the spectrum of adsorbed CO it is crucial that identical spectra can be measured when a sample is sequentially reduced and exposed to CO under identical conditions several times. For our materials this result was most easily achieved by two alternating treatments in H_2 at 523 K and CO (adsorbed near 300 K). Materials reduced just once frequently displayed unusually intense HF bands which could not be reproduced following another reduction. The reasons for this variability are not clear, but separate experiments show it is not directly related to SMSI effects (we focus here on low reduction temperatures), the period of the initial reduction (1 to 20 h), or to metal sintering (we purposely chose poorly dispersed materials for this study to minimize the possible influence of those effects). In any case, the "recipe" described above reliably provided samples whose CO spectra could be reproduced following consecutive reductions at the same temperatures.

RESULTS

Infrared Studies of CO Adsorption

Figure 1 illustrates the time evolution of CO stretching features on sample I at 310 K. This wafer was reduced in flowing H_2 for 22 h at 623 K, evacuated 1 h at 573 K, and cooled to 310 K under vacuum. Twenty torricelli of CO was added and spectra were recorded as a function of time under CO.

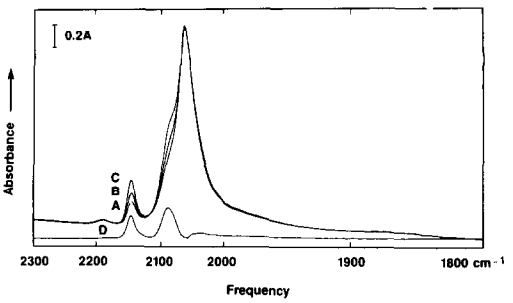

FIG. 1. IR spectrum of sample I reduced at 623 K and evacuated at 573 K under 20 Torr CO at 313 K for (A) 1 min, (B) 10 min, (C) 40 min. Curve (D) is the difference between spectra (C) and (A).

The intensity of the strong band at 2060 cm^{-1} remains constant over the 40-min period, but the bands at 2140 and 2085 cm^{-1} undergo considerable growth as evidenced by the difference spectrum, 1*d*. No significant further development of these bands is observed with longer exposure times. Growth of the 2140- and 2085-cm^{-1} bands is interrupted if gas phase CO is removed after a few minutes exposure. A band at 2180 cm^{-1} is also apparent in Fig. 1. This band disappears upon evacuation and is due to CO weakly adsorbed on dehydroxylated titania sites (*35*).

The chemisorbed CO IR bands intensify further when adsorption is carried out at higher temperatures. Figure 2 contrasts spectra of reduced (523 K; 4 h) and outgassed (He; 623 K; 0.5 h) sample II following 30 min in 20 Torr CO at 310 K and another 10 min in 20 Torr CO at 373 K. Both spectra were measured at 310 K. From the literature we know that the rate of CO disproportionation over Ru is negligible below 400 K (*36–38*). Thus the Boudouard reaction is not responsible for spectral changes observed in the 310 to 380 K regime.

The 2140- and 2085-cm^{-1} bands do not appear when a reduced wafer is treated with subsaturation amounts of CO, as shown in Fig. 3. Here a wafer of II was reduced and outgassed as above and then cooled to 310 K. Spectrum 3a was recorded under vacuum following exposure to 0.2

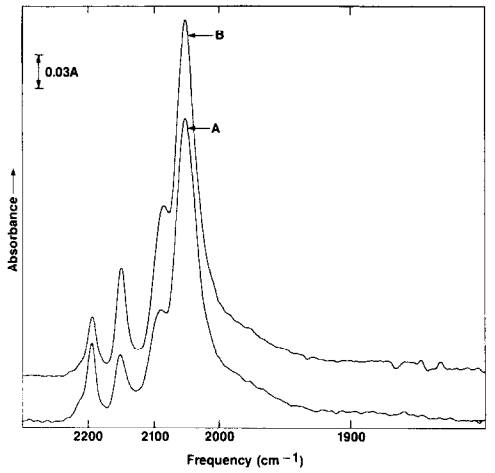

FIG. 2. IR spectrum of sample II reduced and outgassed at 623 K: (A) after 30 min in 30 Torr CO at 313 K, (B) A after 10 min in 30 Torr CO at 373 K. Both spectra were recorded at 313 K.

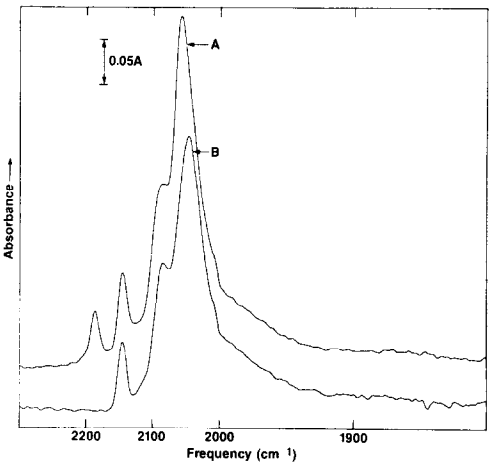

FIG. 4. IR spectrum of I reduced and evacuated at 623 K: (A) after 30 min in 20 Torr CO at 310 K, (B) A after evacuation for 10 min at 310 K.

Torr CO for 5 sec. Spectra 3b–d were also recorded under vacuum after further 5-sec periods in 0.2 Torr CO. Finally, a spectrum of the CO saturated sample is included for comparison. A single CO band grows in intensity and increases in frequency (2020 to 2050 cm^{-1}) at subsaturation coverage. The HF bands at 2140 and 2085 cm^{-1} do not appear until that band is saturated. The formation of the HF bands seems to require a significant CO pressure (at least 1 Torr) in the cell. Once formed in CO, the structures responsible for the HF bands are quite stable in vacuum at 310 K. Figure 4 compares spectra of sample I equilibrated with 30 Torr CO and after evacuation at 310 K for 30 min. The HF bands decline about 5% in magnitude while the 2060-cm^{-1} band redshifts by 10 cm^{-1} under vacuum. These spectral changes are reversed upon readmission of CO.

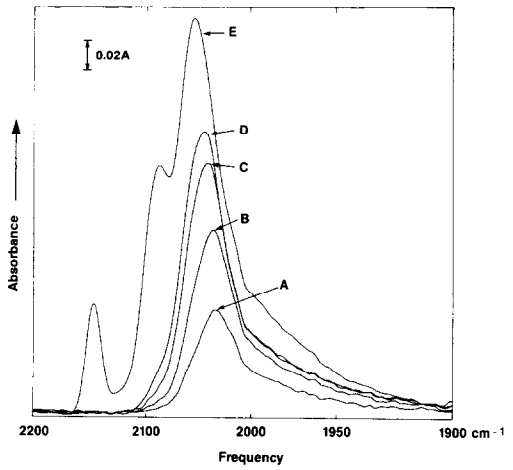

FIG. 3. IR spectra of II reduced at 523 K, outgassed in He at 623 K, then exposed to sequential 0.2 Torr/5 sec doses of CO. (A)–(D) were measured under vacuum following the 2nd, 5th, 8th, and 12th exposures, respectively. (E) shows the sample in 20 Torr CO after 20 min.

Chemisorption of CO also perturbs the shape of the Ru $3d_{5/2}$ XPS line. The spectrum of sample I reduced 2 h at 523 K shows a single peak located near 280 eV (Fig. 5a) which we assign to the Ru $5d_{5/2}$ transition for metallic Ru (*39*). When the sample is then treated with 30 Torr CO for 30 min at 310 K, XPS shows the 280-eV peak is attenuated and a shoulder appears near 282 eV (Fig. 5b). The total area of the Ru $3d_{5/2}$ manifold is unaffected by the CO treatment. The original spectrum in Fig. 5a is fully restored upon reduction in H_2 at 250°C.

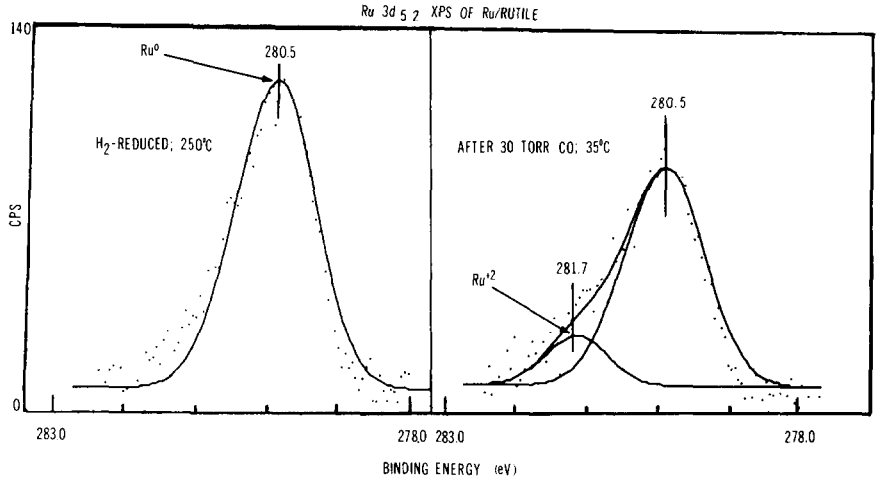

FIG. 5. (A) Ru $3d_{5/2}$ XPS of I recorded under vacuum after 2 h reduction at 523 K. (B) XPS of same material following exposure to 20 Torr CO for 30 min at 310 K.

Exchange and Oxidation of Chemisorbed CO

The Ru–CO surface structures responsible for the 2140-, 2085-, and 2060-cm^{-1} IR bands can be clearly distinguished by their different rates of exchange with isotopically labeled CO and their relative reactivities toward molecular oxygen. When a reduced and ^{12}CO-saturated sample of I or II is evacuated at 310 K and exposed to 20 Torr ^{13}CO, the strong band at 2050 cm^{-1} (under vacuum) shifts to 2003 cm^{-1} (Fig. 6). This value is in accord with that anticipated from the Redlich–Teller rule: $\nu(^{13}C^{16}O) = 0.977\ \nu(^{12}C^{16}O) = 2003\ cm^{-1}$. The sites responsible for the 2140- and 2085-cm^{-1} bands are comparatively inert in this exchange reaction. Weak features near 2080 and 2035 cm^{-1} that could correspond to ^{13}CO species (predicted at 2090 and 2032 cm^{-1}) are occasionally observed, but these may reflect incomplete initial saturation of the HF sites in ^{12}CO. No further exchange of the HF ^{12}CO sites is observed in 30 Torr ^{13}CO at 310 K after 2 h or at 400 K after 10 min.

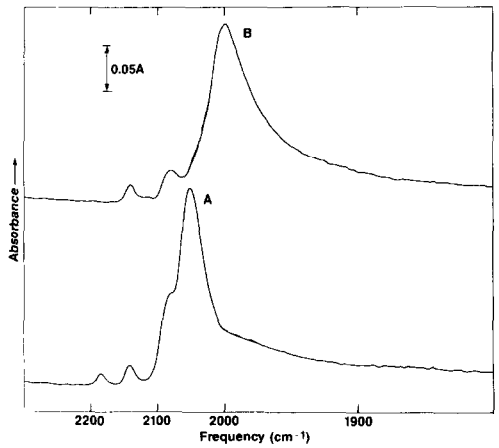

FIG. 6. IR spectrum of reduced and outgassed II after 30 min in 20 Torr ^{12}CO at 313 K. (B) A under 20 Torr ^{13}CO.

Adding 30 Torr O_2 to a CO-saturated and evacuated Ru/TiO_2 wafer at 310 K causes a prompt decline in the intensity of the 2050-cm^{-1} band and the appearance of gas phase CO_2 (Fig. 8). The HF bands are hardly affected by oxygen at 310 K. The 2050-cm^{-1} band disappears entirely as the wafer is heated in O_2 to 400 K. Complete extinction of the HF bands requires heating the wafer in 30 Torr O_2 to 425 K.

The structure responsible for the 2060-cm^{-1} band is the only one that easily exchanges with gas phase CO. This selective exchange provides a means to quantify the

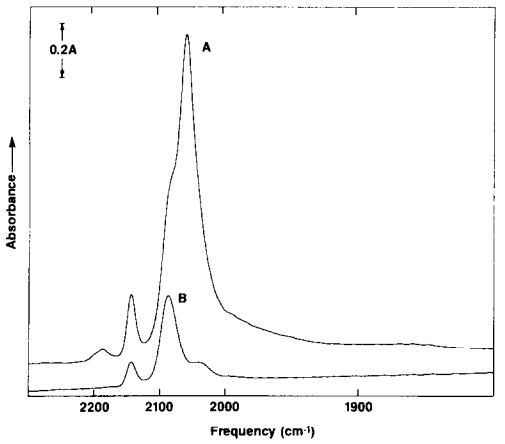

FIG. 7. IR spectrum of I under 20 Torr CO following reduction and evacuation at 623 K. (B) Same sample under vacuum after evacuation and exposure to 20 Torr O_2 for 10 min at 313 K.

distribution of CO among the HF and 2060-cm^{-1} sites. To accomplish this, a wafer of reduced and outgassed II was saturated in 20 Torr ^{12}CO for 40 min at 310 K. The sample was next evacuated (20 min) and exposed to 5 Torr ^{13}CO for 3 min. The evacuation/^{13}CO exposure sequence was repeated three more times to ensure complete labeling of the exchangeable surface species. IR spectra confirmed the HF bands did not exchange with the labeled CO. Forty torricelli O_2 was added to the evacuated cell which was then heated to 425 K and held there 15 min. IR spectra measured at this point confirmed complete elimination of surface carbonyl species. The gas inside the cell was released into the vacuum manifold and analyzed mass spectrometrically. Based on the intensity ratios at *m/e* 44/(45 + 47), (i.e., $^{12}C^{16}O_2/(^{13}C^{16}O_2 + {}^{13}C^{16}O^{18}O)$ and *m/e* 12/13 we conclude that 25 ± 2% of the bound CO for the sample depicted in Fig. 7 was on HF sites. That value was confirmed in another experiment on the same sample where the labeling scheme was reversed. A blank experiment where no CO was introduced produced less than 1% of the CO_2 detected in the CO oxidation studies. However, we should point out that achieving this necessary result required three cycles through a treatment involving oxidation (O_2; 473 K; 2 h) and reduction (H_2; 523 K; 2 h). This procedure eliminated adventitious surface carbon whose presence initially biased the $^{12}CO_2$ content.

To determine if the 2085- and 2140-cm^{-1} bands are coupled vibrations due to $Ru(CO)_x$ ($x > 1$) sites, we examined IR spectra of I saturated with mixtures of ^{12}CO and ^{13}CO. A single wafer was employed in this sequence and a standard pretreatment involving reduction in H_2 (523 K; 1 h) and evacuation (523 K; 1 h) was used prior to soaking the sample in 10 Torr of premixed $^{12}CO/^{13}CO$ for 30 min. The 2150- to 2070-cm^{-1} region of spectra measured in 0, 20, 40, 60, and 99% ^{13}CO are shown in Fig. 8. We focus on this spectral region because it allows us to track the evolution of the band that appears at 2140 cm^{-1} in pure ^{12}CO and at 2092 cm^{-1} in pure ^{13}CO. In 60% ^{12}CO the 2140-cm^{-1} feature is poorly resolved, but a peak at 2134 cm^{-1} and a shoulder near 2120 cm^{-1} are evident. The 2134-cm^{-1} peak becomes progressively weaker as the ^{12}C is diluted to 40 and then 20%. A well-resolved peak develops at 2120 cm^{-1} in 20% ^{12}CO. A shoulder near 2090 cm^{-1} is apparent in 40%

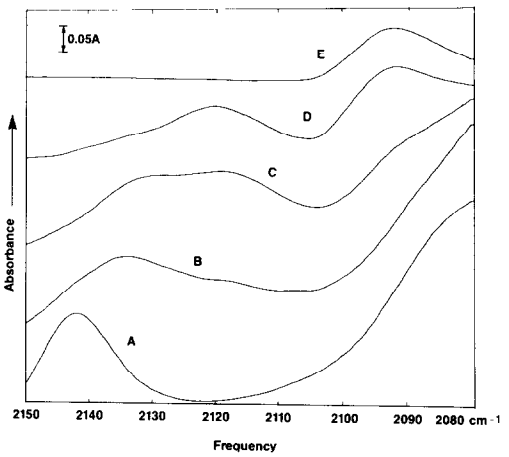

FIG. 8. IR spectra of I reduced and evacuated at 523 K in 10 Torr CO with increasing enrichment in ^{13}CO. (A) 99% ^{12}CO; (B) 60% ^{12}CO; (C) 40% ^{12}CO; (D) 20% ^{12}CO; (E) 1% ^{12}CO.

^{12}CO and develops into a resolved peak at 2092 cm^{-1} at higher ^{13}CO concentrations.

DISCUSSION

Assignment of the 2060-cm^{-1} Band

The 2060-cm^{-1} band which dominates the spectrum of CO on Ru/TiO_2 is readily assigned to CO chemisorbed on Ru particles. Vibrational studies of CO on Ru(001) show a single C–O vibrational band increasing in frequency from 1984 to 2060 cm^{-1} as the CO coverage increases from 0.003 to 0.66 (*22*). While we could neither calibrate our coverages nor guarantee a homogenous distribution of CO across the thickness of our wafers, the spectra shown in Fig. 3 also show a monotonic growth and blue shift as CO coverage increases. In fact the persistence of a low-frequency (ca. 1980 cm^{-1}) should in our "coverage" set suggests the presence of Ru particles with comparatively low CO coverage. Such a situation could arise because of preferential CO adsorption (and saturation) near the wafer surface vs the porous wafer interior. High-resolution infrared reflection–absorption spectra of CO on Ru(001) exhibit bandwidths four times narrower than we find here, even at saturation coverages (*40*). That implies our supported systems present Ru facets other than the (001) orientation, as might be expected for small Ru particles. CO desorbs at a negligible rate from Ru(001) at 310 K, but it is rapidly displaced from the surface by gas phase CO at sub-Torr CO pressures (*41*). Our supported systems exhibit the same behavior, suggesting that the exchange reaction occurs via a CO displacement rather than Ru–CO dissociation mechanism. The displacement reaction could be facilitated by the intermixing of CO among strongly and weakly bound adsorption states (*42*). The population of more weakly bound states at high CO pressures is evidenced by the reversible 10-cm^{-1} shift observed when spectra of CO on Ru/TiO_2 are compared under vacuum and under CO (Fig. 4).

At low levels of exposure under UHV conditions, molecular O_2 will displace and possibly oxidize a portion of a CO monolayer on Ru(001). CO remains strongly coadsorbed with O on Ru at an O coverage of 0.33 and exhibits a CO stretching frequency of 2080 cm^{-1} in this state (*24*). When exposed to O_2 at higher temperatures and pressures, a thicker oxide forms on Ru which does not chemisorb CO at ambient temperature. Again these results are in agreement with our and others findings for CO on supported Ru particles. CO on mildly oxidized Ru shows an IR band at 2080 cm^{-1}. More exhaustive oxidation yields surfaces that will not adsorb CO at 310 K.

Assignment of the 2140- and 2085-cm^{-1} Bands

On the basis of their chemical and spectroscopic properties, we assign the 2140- and 2085-cm^{-1} IR bands to coupled vibrations arising from surface-grafted $(TiO)_x Ru(CO)_n$ species where x is probably 2 and n is likely 2 or 3, depending on the degree of aggregation. Figures 1 and 2 show the HF bands develop in CO with constant stretching frequencies. This is consistent with the formation of discreet molecular entities on the surface. The IR spectra measured in mixtures of ^{12}CO and ^{13}CO (Fig. 8) show the 2140- and 2085-cm^{-1} vibrations are coupled. The behavior of the 2085-cm^{-1} band is difficult to track in these experiments as it overlaps strongly with the stronger metallic Ru–CO band at 2003 to 2060 cm^{-1}. However, a crude analysis of the higher frequency component allows us to draw some conclusions regarding the structure of this polycarbonyl site. First, the 2140-cm^{-1} band cannot be due to an isolated $Ru–CO^{x+}$ species. This type of site would give rise to only two bands with varying relative intensities when formed in mixtures of ^{12}CO and ^{13}CO. We can also rule out vibrationally isolated $Ru(CO)_2^{n+}$ sites. Three high-frequency components are expected for mixtures of $Ru(^{12}CO)_2$, $Ru(^{13}CO)(^{12}CO)$, and $Ru(^{13}CO)_2$ (as are found in the case of alumina–O–$Rh(CO)_2$ sites), but we find at least

four. A more complete spectra deconvolution could yield even more high-frequency components.

Isolated $Ru(CO)_n^{x+}$ ($n > 2$) sites are viable candidates. For an $Ru(CO)_3$ site with C_{3v} symmetry we expect two IR bands in monoisotopic CO and a total of 10 bands as the $^{12}CO/^{13}CO$ ratio is varied. We cannot rule out oligomeric structures such as $[Ru^{x+}(CO)_2]_y$. Halide bridged polymers with this formula are known and coupling between adjacent $Ru(CO)_2$ oscillators could yield complex vibrational spectra in isotopic mixtures of CO.

The conclusion that the HF bands arise from formally oxidized Ru sites is based on chemical and spectral analogy to know molecular Ru species as well as XPS results. The XPS data show a fraction of the zero-valent Ru on a reduced specimen is converted to a more oxidized form when CO is added. The 2140-cm^{-1} IR band is 80 cm^{-1} higher in frequency than that found for CO on metallic Ru. High-frequency CO bands such as those found here are usually associated with metal carbonyl halides which, in the case of Ru, form a very diverse class of stable structures with Ru in a variety of oxidation states. Seddon and Seddon have tabulated IR data for nearly a hundred such compounds in a recent text (*26*). Of these, only the halide bridged dimers, $Ru_2(CO)_6X_4$, exhibit a pair of IR bands near 2140 and 2085 cm^{-1} (X = Cl: 2143, 2083 cm^{-1}; X = Br: 2137, 2078 cm^{-1}). We previously showed that IR spectra of alumina-bound Al–O–$Rh(CO)_2$ moieties are very similar spectroscopically to molecular species like the Cl-bridged $[Rh(CO)_2Cl]_2$ in solution (*31*). This implies the electron donor properties of surface oxides acting as ligands for cationic metal centers can resemble those of a halide. This spectral similarity leads us to favor the formulation $[(TiO)_2Ru(CO)_3]_n$ as a representation of the structure that generates the HF IR bands. Here, TiO refers to an oxygen anion on the titania surface. The quantity n is left undefined in recognition of the fact that halide bridged molecular dimers like those described above can coordinate to weak oxygen bases to yield monomeric products whose IR spectra are strikingly similar to their parents' (*43*). On oxide surfaces it is conceivable that adsorbed water or hydroxyl groups could fulfill a similar role.

In the light of this structural paradigm, it is not surprising that the surface-grafted species are inert with respect to oxygen and CO exchange. The proposed molecular analogs are stable in air as solids and in solution. They are 6-coordinate, $18e^-$, closed shell species with notoriously high barriers to ligand replacement via associative or dissociative mechanisms. In contrast, surface grafted $Rh(CO)_2^+$ species undergo rapid exchange with gas phase CO at room temperature. Their molecular analogs possess a closed shell $18e^-$ configuration too, but they possess an open coordination site and CO replacement can occur by an associative mechanism (*44*).

A Model for $[(TiO)_2Ru(CO)_3]_n$ *Formation*

If our structural description is correct, it is important to address the question how are such oxidized Ru sites formed on allegedly well-reduced materials. We considered three possibilities. First, the hydrogen reduction is incomplete, leaving a portion of the Ru as an oxidized surface titanate. Second, CO dissociates on Ru to leave oxide and carbide. The oxide migrates to oxygen vacancies on the titania and forms bonds with Ru when CO is added. Third, the Ru is initially fully reduced, but interacts with CO and surface hydroxyl groups in a redox process to yield oxidized $(TiO)_x$ $Ru(CO)_n$ centers and H_2.

The first case is worth considering because many early and first-row transition metals form very stable surface aluminates, silicates, titanates, etc., that reduce to their metallic state only at temperatures well above those required to reduce the bulk metal oxide to metal. XPS evidence argues against this notion. The spectra in Fig. 5 show the high binding energy Ru species are generated only when CO is added to the

Ru/TiO_2 at 310 K. Other experiments show the HF bands form even when the samples are reduced at 700 K.

We consider the second possibility because it is known that some CO dissociates upon contact with Fe, Ru's first row neighbor, at room temperature. This is unlikely for several reasons. CO chemisorption has been studied in detail on several Ru cyrstallographic planes, but its dissociation near 300 K has not been reported (*45–48*). The spontaneous dissociation of CO should leave behind a surface carbide. Solid state NMR spectra of CO on supported Ru do show evidence for diamagnetic polycarbonyl structures, but not carbides (*49, 50*).

We prefer the third model which posits that chemisorption of CO can induce a redox reaction between metallic Ru and surface hydroxyl groups on the support. This type of reaction, represented by Eqs. (1) and (2) in the Introduction, is driven by thermodynamic forces. As Prins *et al.* noted, the average metal–metal bond enthalpy (99 kJ $mole^{-1}$ for Rh, 108 kJ $mole^{-1}$ for Ru) is only about half of the average metal–CO bond enthalpy (185 kJ $mole^{-1}$ for Rh, 180 kJ $mole^{-1}$ for Ru) (*30, 33*). As a consequence, the molecular carbonyls of Fe, Co, Ni, Rh, Ru, Ir, and Os all have large negative standard free energies of formation at room temperature (*33, 51*). The rate of $M(CO)_x$ generation from the reaction of bulk metal with CO varies widely among these metals. For Ni the rate is so rapid, the reaction is the basis of an industrial process for production of high purity metal powders (*52*). The rate is at best slow for the other metals at room temperature and near-atmospheric CO pressures, but those rates must reflect kinetic, not thermodynamic, limitations. Pichler noted the presence of soluble Ru carbonyls in the products of high-pressure CO-hydrogenation over Ru black in 1963 (*53*). More recently, Goodwin *et al.* and Kobayashi have shown $Ru(CO)_5$ and $Ru_3(CO)_{12}$ are formed when reduced Ru/silica is contacted with 1 atm CO at 300 to 473 K (*54*). These observations show that the carbonylation of Ru is both favored thermodynamically and feasible kinetically under our experimental conditions.

It is difficult to estimate the energetics involved in the proposed redox process involving the formation of TiO–Ru bonds and the elimination of H_2. However, many studies show that even coordinatively saturated zero-valent Ru carbonyl compounds undergo CO loss and oxidation upon contact with hydroxylated supports at temperatures ranging from 300 to 500 K (*12, 25–29*). Our experimental data do not allow us to discern whether the proposed $(TiO)_2Ru(CO)_3$ species form in the concerted reaction of Ru with hydroxyl groups and CO or in a two-step process with initial carbonylation of Ru and subsequent oxidation and grafting of the gas phase carbonyl. We merely wish to point out that the proposed oxidative fragmentation reaction is a viable one because the steps of the two-stage reaction proceed spontaneously at or near our reaction conditions.

The observation that some HF species form promptly upon addition of CO at 310 K while others form more slowly may reflect the structural heterogeneity of Ru atoms on a supported catalyst. We might expect the oxidative fragmentation reaction to proceed rapidly for those Ru atoms with the fewest bonds to other Ru atoms and the closest proximity to the oxide surface. Such atoms will be found in the smallest metal particles or at the edges of larger ones. At the other extreme, we anticipate that Ru atoms in the core of large metal particles would not undergo the reaction unless the oxidative fragmentation process removed neighboring metal atoms and exposed them to the gas phase and oxide surface. Many intermediate structural environments are conceivable and may be responsible for the sites that generate HF IR bands slowly at 310 K.

ACKNOWLEDGMENTS

I am indebted to Ms. N. Dudash for performing some of the IR measurements and to Mr. John Hardenbergh and Dr. Dan Dwyer for measuring the photoelectron spectra.

REFERENCES

1. Yang, C.-H., and Goodwin, J. G., Jr. *J. Catal.* **78,** 182 (1982).
2. Dalla Betta, R. A., *J. Phys. Chem.* **79,** 2519 (1975).
3. Kobayashi, M., and Shirasaki, T., *J. Catal.* **28,** 289 (1973).
4. King, D. L., *J. Catal.* **51,** 386 (1978).
5. Chen, H. W., Zhong, Z., and White, J. M., *J. Catal.* **90,** 119 (1984).
6. Brown, M. F., and Gonzalez, R. D., *J. Phys. Chem.* **80,** 1731 (1976).
7. Abhivantanapon, P., and Gardner, R. A., *J. Catal.* **27,** 56 (1972).
8. Cant, N. W., and Bell, A. T., *J. Catal.* **73,** 257 (1982).
9. Davydov, A. A., and Bell, A. T., *J. Catal.* **49,** 332 (1977).
10. Schwank, J., Parravano, G., and Gruber, H. L., *J. Catal.* **61,** 19 (1980).
11. Guglielminotti, E., Spoto, G., and Zecchina, A., *Surf. Sci.* **161,** 202 (1985).
12. Kuznetsov, V. L., and Bell, A. T., *J. Catal.* **65,** 374 (1980).
13. Kimura, T., Okuhara, T., Misono, M., and Yoneda, Y., *J. Chem. Soc. Japan* **2,** 162 (1982).
14. Guglielminotti, E., Zecchina, A., Bossi, A., and Camia, M., *J. Catal.* **74,** 252 (1982).
15. Guglielminotti, E., *Langmuir* **2,** 812 (1986).
16. Kiss, J. T., and Gonzalez, R. D., *J. Phys. Chem.* **88,** 892 (1984).
17. Goodwin, J. G., Jr., and Naccache, C., *J. Catal.* **64,** 482 (1980).
18. Winslow, P., and Bell, A. T., *J. Catal.* **86,** 158 (1984).
19. Kellner, C. S., and Bell, A. T., *J. Catal.* **75,** 251 (1982).
20. Miura, H. M., McLaughlin, M. L., and Gonzalez, R. D., *J. Catal.* **79,** 227 (1983).
21. Kellner, C. S., and Bell, A. T., *J. Catal.* **71,** 296 (1981).
22. Pfnur, H., Menzel, D., Hoffmann, F., Ortega, A., and Bradshaw, A. M., *Surf. Sci.* **93,** 431 (1980).
23. A pair of bands at lower frequency (2040 and 1960 cm^{-1} in Ref. (*21*)) is also observed sometimes. A band at 1950 cm^{-1} is occasionally reported for CO on reduced, supported Ru (Ref. (*15*)).
24. Thomas, G., and Weinberg, W., *J. Chem. Phys.* **70,** 954 (1979).
25. Iwasawa, Y., *in* "Advances in Catalysis" (D. D. Eley, P. W. Selwood, and P. B. Weisz, Eds.), Vol. 35, p. 187. Academic Press, San Diego, 1987.
26. Seddon, E. A., and Seddon, K. R., *in* "The Chemistry of Ruthenium," Chaps. 8–11. Elsevier, Amsterdam/New York, 1984.
27. Zecchina, A., Guglielminotti, E., Bossi, A., and Camia, M., *J. Catal.* **74,** 225 (1982).
28. Schay, Z., Lazar, K., Mink, J., and Guczi, L., *J. Catal.* **87,** 179 (1984).
29. Evans, J., and McNulty, G. S., *J. Chem. Soc. Dalton Trans.*, 1123 (1984).
30. Van't Blik, M., Van Zon, J., Huizinga, T., Koningsberger, D., and Prins, R., *J. Phys. Chem.* **87,** 2264 (1983).
31. Robbins, J. L., *J. Phys. Chem.* **90,** 3381 (1986).
32. Solymosi, F., and Pasztor, M., *J. Phys. Chem.* **89,** 4789 (1985).
33. Connor, J. A., *Top. Curr. Chem.* **71,** 71 (1977).
34. Dwyer, D. J., and Hardenbergh, J. H., *J. Catal.* **87,** 66 (1984).
35. Yates, D. J. C., *J. Phys. Chem.* **65,** 746 (1961).
36. Rabo, J. A., Risch, A. P., and Poutsma, M. L., *J. Catal.* **53,** 295 (1978).
37. Low, G. G., and Bell, A. T., *J. Catal.* **57,** 397 (1979).
38. Yamasaki, H., Kobori, Y., Naito, S., Onishi, T., and Tamaru, K., *J. Chem. Soc. Farad. Trans. 1* **77,** 2913 (1981).
39. Muielenberg, E., *in* "Handbook of X-Ray Photoelectron Spectroscopy." Perkin-Elmer Corp., 1979.
40. Hoffmann, F. M., and Persson, B. N. J., *Phys. Rev. B* **34,** 4354 (1986).
41. Yamada, T., and Tamaru, K., *Surf. Sci.* **146,** 341 (1984).
42. Shanahan, K. L., and Muetterties, E. L., *J. Amer. Chem. Soc.* **88,** 1996 (1984).
43. Johnson, B. F. G., Johnston, R. D., and Lewis, J., *J. Chem. Soc. A*, 792 (1969).
44. Wang, H. P., and Yates, J. T., Jr., *J. Catal.* **89,** 79 (1984).
45. Pfnur, H., Feulner, P., and Menzel, D., *J. Phys. Chem.* **79,** 4613 (1983).
46. Fuggle, J. C., Umbach, E., Feulner, P., and Menzel, D., *Surf. Sci.* **64,** 69 (1977).
47. Reed, P. D., Comrie, C. M., and Lambert, R. M., *Surf. Sci.* **59,** 33 (1976).
48. Goodman, D. W., Maddey, T. E., Ono, M., and Yates, J. T., Jr., *J. Catal.* **50,** 279 (1977).
49. (a) Duncan, T. M., Winslow, P., and Bell, A. T., *Chem. Phys. Lett.* **102,** 163 (1983); (b) Duncan, T. M., and Root, T. W., *J. Phys. Chem.* **92,** 4426 (1988).
50. (a) Gay, I. D., *J. Magn. Res.* **58,** 413 (1984); (b) Shoemaker, R. K., and Apple, T. M., *J. Phys. Chem.* **89,** 3185 (1985).
51. Behrens, R. G., *J. Less-Common Met.* **56,** 55 (1977).
52. Mond, L., Langer, R., and Quincke, E., *J. Chem. Soc.* **57,** 749 (1890).
53. Pichler, V. H., and Firnhaber, B., *Brennst.-Chem.* **44,** 13 (1963).
54. Goodwin, J. G., Jr., Goa, D. O., Erdal, S., and Rogan, F. H., *Appl. Catal.* **24,** 199 (1986).
55. Kobayashi, M., *J. Catal.* **92,** 184 (1985).